Fast quantitative elemental mapping of highly inhomogeneous materials by micro-Laser-Induced Breakdown Spectroscopy

S. Pagnotta[a,b*], M. Lezzerini[b], B. Campanella[a], G. Gallello[d], E. Grifoni[a], S. Legnaioli[a], G. Lorenzetti[a], F. Poggialini[a], S. Raneri[b], A. Safi[c], V. Palleschi[a]

[a] Applied and Laser Spectroscopy Laboratory, Institute of Chemistry of Organometallic Compounds, Research Area of National Research Council, Via G. Moruzzi, 1 – 56124 Pisa, Italy
[b]Department of Earth Sciences, University of Pisa, Via Santa Maria 53, Pisa, Italy
[c]Laser and Plasma Research Institute, Shahid Beheshti University, G. C., Evin, Tehran, 1983963113 Iran
[d]Department of Archaeology, University of York, King's Manor, YO17EP York, UK

Abstract

In this work, a fast method for obtaining a quantitative elemental mapping of highly inhomogeneous samples by μ-LIBS maps is proposed. The method, transportable and cheap, allows the analysis of large maps through the use of a Self-Organizing Map clustering method coupled to Calibration-Free LIBS for quantification of cluster prototypes. The method proposed has been verified on heterogeneous materials such historical lime mortars but it can be easily applied to a larger class of inhomogeneous materials for very different applications (modern building materials, biological samples, industrial materials, etc.).

Keywords: LIBS, Elemental Mapping, Calibration-Free LIBS, Self-Organizing Maps, Mortars

* *Corresponding author:* stefanopagnotta@yahoo.it

1. Introduction

Laser-based techniques have attracted a considerable interest in the last decades for their capability of obtaining elemental images of solid samples without specific treatment, with high spatial resolution and at different depths [1-5]. A number of applications have been proposed in several fields, ranging from biomedical, geological and environmental research, to forensic analysis, to industrial diagnostics, to Cultural Heritage study and conservation [6-13].

Among these techniques, applications based on the μ-LIBS technique are becoming more and more frequent to scan surfaces and obtain compositional maps, providing interesting results in a number of applications that require qualitative and quantitative analyses [14-22]. The use of μ-LIBS-scan technique has proved to be very advantageous from an economic and experimental point of view with respect to other laser-based techniques such as Laser-Ablation-Inductively Coupled Plasma-Mass Spectrometry (LA-ICP-MS) [23]. The method is, in fact, fast, transportable, relatively cheap and can analyse simultaneously elements with very different ionization energy, a task that can be problematic in LA-ICP-MS [24]. While the qualitative analysis of μ-LIBS elemental maps is a relatively simple task, the quantification of the elemental composition of the sample is much more challenging. In principle, a quantitative analysis based on the use of reference samples of known composition for building linear or non-linear, uni- or multi-variate calibration surfaces is applicable only when the matrix of the sample remains more or less constant in the region of analysis [25]. If the sample is characterized by strong inhomogeneities, with materials of different matrixes, or when suitable reference samples are not available, a possible approach to quantitative elemental mapping would be the use of Calibration-Free approaches [25-27]. An important drawback of the CF-LIBS approach, however, is the time required for the analysis: the emission lines of the elements in the samples must be individuated and their intensities calculated through their fit with a Voigt profile. The electron number density must be calculated from the Stark broadening of the hydrogen Balmer alpha line, then the electron temperature must be calculated from the Boltzmann or Saha-Boltzmann plot. Finally, the sample composition must be calculated. If automated all these operations take at least less than 30 seconds per spectrum; however, μ-LIBS elemental maps with megapixel spatial resolution have been obtained by different groups, and a CF-LIBS approach applied on millions of LIBS spectra is, at the moment, unrealistic. D'Andrea et al. [28] have recently proposed a hybrid Artificial Neural Network (ANN) – CF-LIBS method that can be very effective in most of the cases, but requires the variations in the material matrix to be relatively small for the ANN to work properly.

In this work, we propose a method based on the sequential application of elemental map segmentation (obtained using an automatic classification method based on the use of Self-Organizing Maps, as

proposed by the authors in [29]), followed by a CF-LIBS analysis of the prototypal spectra representing the different clusters (materials) in the map. The method is presented and tested for the analysis of ancient mortars. The knowledge developed in the study of this class of highly inhomogeneous materials may have also interesting applications in the analysis and study of modern binding materials and techniques.

2. Materials and methods

To assess the analytical capability of the method proposed, two mortar fragments from the Norman Adrano Castle (Catania, Sicily) were selected as test samples. The two samples (labelled with the inventory numbers N2-2 and S2-3) have been analysed with the permission of the *Soprintendenza per i Beni culturali e Ambientali di Catania*. They consist of polished thin sections consolidated by epoxy resin; the mortars are characterized by a heterogeneous binder with the presence of aggregates due to volcanic ash, with a large variation in grain size (figure 1).

The analysis of ancient mortars is one of the main topics of Earth Sciences disciplines applied to Cultural Heritages. Usually, ancient mortars are classified in two main categories, lime-aerial mortars and hydraulic lime mortars. The latter ones were often obtained by adding to the mixtures volcanic materials ("pozzolana"), and crushed ceramic fragments ("cocciopesto"). In both cases, the final product is a mixture characterised by a relatively homogeneous paste, embedding inside clasts of various dimension. The ability of pozzolanic materials to provide hydraulic proprieties to the mortars is due to the presence of reactive constituents like aluminates and silicates [30]. A quantitative elemental mapping could thus give information about the typology of analyzed mortars (aerial vs. hydraulic) and well as the degree of hydraulicity (Vicat formula [31]). Usually, the characterization of ancient mortars is achieved by optical microscopy (OM), X-ray fluorescence (XRF), X-ray diffraction (XRD), scanning electron microscope (SEM-EDS), termogravimetric methods [32] and inductively coupled plasma mass spectrometry (ICP-MS) [33]. However, from an analytical point of view, the heterogeneity proper of these kind of materials and the presence of low crystalline CSH (Calcium-Silicate-Hydrated) phases [34,35] represent, sometimes, a limit for the complete characterization of mortars, especially considering the difficult to delineate the spatial distribution and the occurrence of CSH with respect to binder and aggregates.

An interesting method based on semi-automated algorithm working on elementary maps obtained by SEM-EDS data has recently been proposed by Belfiore et al. [36].

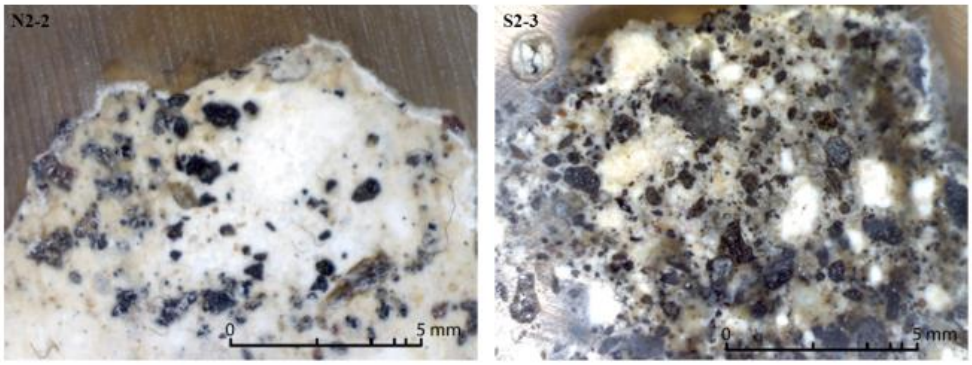

Figure 1. Microphotography of the two mortar samples.

3. Experimental procedure

A μ-Modì double-pulse instrument [37], equipped with a collinear double-pulse Nd:YAG Laser (λ=1064 nm) coupled with a Zeiss Axio Plan A1 microscope with 10X objective was used for the mapping of the samples. The energy of the two pulses was set to 20 mJ and 30 mJ, respectively, in 20 ns FWHM [38]. The delay between the laser pulses was set at 1μs. The LIBS signal was collected using an optical fiber, placed at 45° with respect to the laser direction, at a distance of about 1 cm from the sample. A ball lens in front of the fiber guarantees the optimal collection of the LIBS signal from the whole plasma. The μ-Modì instrument uses an Avantes double spectrometer (AvaSpec-2048-2), covering the spectral region from 190 to 900 nm (0.1 nm resolution from 190 to 450 nm, 0.3 nm resolution from 450 to 900 nm). The spectra were acquired 250 ns after the second laser pulse. The acquisition time of the spectrometer is of about 2 ms (time-integrated measurements). The samples were placed on a motorized X-Y sample holder, synchronized with the laser and spectrometer through a LabVIEW® dedicated software. The element maps were acquired on a 50x50 matrix (2500 LIBS spectra) with a lateral resolution of 100 μm, for a total scanned area of 25 mm^2, with the laser operating at 1 Hz repetition rate. The diameter of the laser crater at the sample surface was about 20 μm [29].

The main elements present in the mortars are reported in table I, along with the central wavelength of the emission line used for building the compositional images from the LIBS spectra. Given the qualitative nature of the analysis, at this stage, the use of self-absorbed resonant lines is tolerable.

Table I - Selected elements and central wavelength of the line considered

Element	Ion.	λ(nm)
C	I	247.8
Na	I	589.0
Mg	II	279.4
Al	I	309.3
Si	I	288.2
Fe	I	372.0
Ca	I	445.2

4. Results

Based on the intensity of the lines identified, a series of elementary maps constituting the starting point for the subsequent clusterization (or segmentation) processing were obtained, as shown in figure 2.

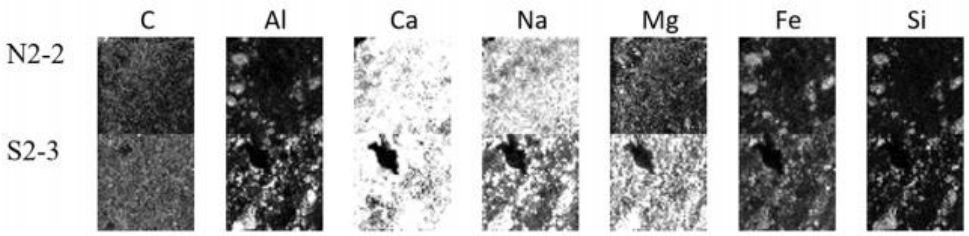

Figure 2. The elemental maps obtained by μ-LIBS scan

Following the method described in ref. [29], for the qualitative characterization of the spatial relationship between aggregate and binder we realized for both the samples a grayscale map of the Ca/Mg line intensity ratio and a false-color map of the distribution of Si (red), Al (green) and Ca (blue) line intensity (see figure 3).

The Ca/Mg ratio maps allow us to easily discriminate the distribution of binder (dark areas) and aggregates present in mortar (bright areas). The Si-Al-Ca false-color maps evidence further the high inhomogeneity of the samples.

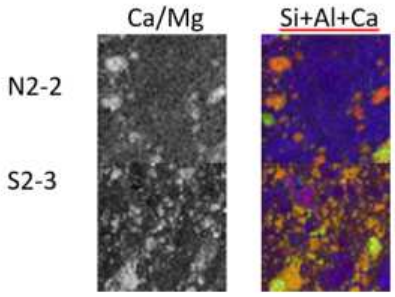

Figure 3. At the left, the map representing the Ca/Mg line intensity ratio. At the right, the false-color map representing the distribution of Si (red), Al (green) and Ca (blue) line intensity.

Although clear from a qualitative point of view, the differences in the sample matrix from point to point prevent the possibility of using a unique calibration strategy based on the construction of univariate calibration curves or multivariate linear (Partial Least Square Analysis, for example) or non-linear (Artificial Neural Networks) approaches.

The first step of our proposed analytical strategy is thus the automatic segmentation of the elemental images using a Self-Organizing Map neural network [39], with the purpose of detecting and separating the different components in the samples.

The SOM network is an unsupervised neural network that consists of neurons organized in a low-dimensional network. Each neuron is represented by an n-dimensional weight vector where n is the number of dimensions of the input vectors (in our case, n=7, corresponding to the peak intensity of the lines reported in table I). The input vectors are normalized to have unit length. The samples (in our case, the set of LIBS spectra defining the 'pixels' of the image) are assigned to the nodes whose weights are 'closer' to their LIBS spectra. The different neurons adjust their weights in order to get the largest possible number of samples, in a competitive way.

The use of SOM networks is suitable for detecting the topology of samples [40-41] and, at the same time, operating in a multidimensional parameters space without reducing the dimensionality of the system [42]. Since the number of different materials in the mortars is not known a priori, we chose a 5-neuron SOM which will select a maximum of 5 independent clusters (figure 4). These clusters should well represent the inhomogeneity of the sample. Given the unavoidable slight experimental differences between the two acquisitions, each sample was segmented independently on the other.

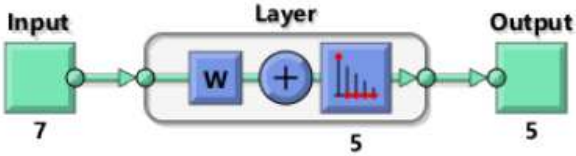

Figure 4. The network scheme: 7 inputs (peak line intensities), 5 segments as output.

Five segments for each sample was therefore obtained (figure 5). Each image obtained from SOM segmentation represents materials with similar composition/matrix [29].

	Seg. 1	Seg.2	Seg.3	Seg.4	Seg.5
N2-2					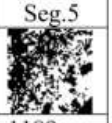
pixel	238	309	20	744	1189
S2-3				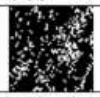	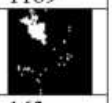
pixel	523	677	682	455	163

Figure 5. Image segmentation produced by the SOM neural network with the number of pixels represented.

In both the mortar samples studied, the SOM segmentation reproduces similar patterns, although not corresponding to the same cluster number. For example, the regions of the samples where the epoxy resin used for consolidating the samples is exposed are clearly evidenced in segment 3 for sample N2-2 and segment 5 for sample S2-3.

As an interesting by-product of this classification, the area covered by each material can be estimated by the ratio between the pixel associated with a given cluster and the total number of pixels of the map. While the surface exposed in sample N2-2 is negligible (20 pixels over 2500 = 0.8 %), the corresponding exposed surface on sample S2-3 corresponds to 163 pixels over 2500 = 6.5 %.

It is evident that averaging the LIBS spectra over the whole map would give unreliable results, that would be strongly affected by the amount of clasts, the exposed epoxy resin, etc., in the scanning area. Thus, the quantitative determination of the composition of the samples must be done separately for the different clusters/materials evidenced by the SOM classification. As discussed in [29], the SOM segmentation gives the 'coordinates' (normalized peak line intensities, since the input vectors are normalized to have unit length) of the centroids of the clusters (see figure 6). However, the centroids of the clusters do not necessarily coincide with the coordinates of a 'pixel' of the image. In

other words, the corresponding intensities does not match any physical LIBS spectrum, so this information cannot be used for a Calibration-Free quantitative analysis.

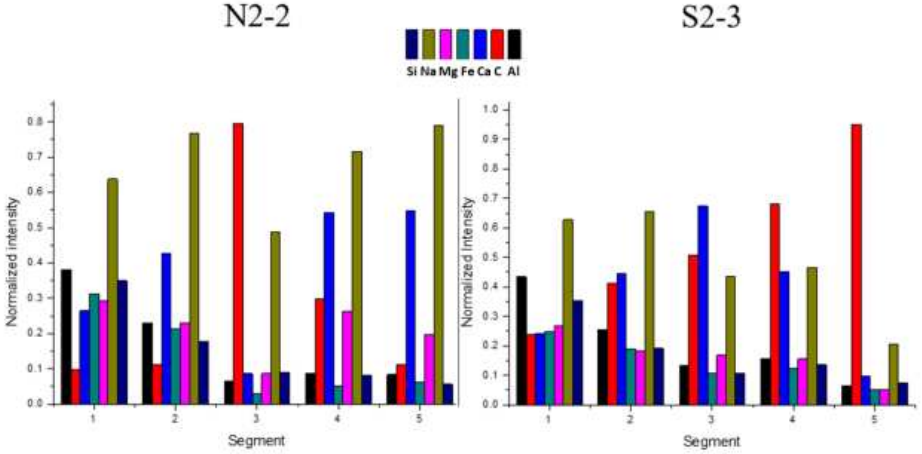

Figure 6 – Normalized intensities corresponding to the centroid of the distribution.

On the other hand, the materials corresponding to each cluster have a homogeneous distribution within the cluster, therefore we can average the spectra corresponding to each cluster and apply the CF-LIBS method to these spectra only, obtaining the quantitative composition of the materials in the sample.

The emission lines considered for the quantitative analysis are reported, with the corresponding spectral parameters, in table II. The lines were chosen trying to avoid strong self-absorbed emissions, whenever possible.

Table II - Emission lines used for the CF-LIBS analysis and their relevant spectral parameters

Element	Ion.	Wavelength (nm)	E_k (x10^{-4} cm^{-1})	A_{ki} (x10^{-8} s^{-1})	g_k
Al	I	237.31	4.22	0.81	6
Fe	II	238.20	4.2	3.8	12
Fe	II	239.56	4.21	2.5	10
Fe	II	239.92	4.23	1.4	6
C	I	247.85	6.2	0.18	3
Si	I	250.69	4.0	0.47	5
Si	I	251.61	4.0	1.21	5
Si	I	251.92	3.98	0.46	3
Si	I	252.41	3.97	1.82	1
Si	I	252.85	3.98	0.77	3
Fe	II	258.58	3.87	0.81	8

Fe	II	259.94	3.85	2.2	10
Fe	II	260.65	7.46	1.8	6
Mg	I	285.21	3.51	4.91	3
Si	I	288.15	4.1	1.89	3
Al	I	308.21	3.24	0.63	4
Al	I	309.27	3.24	0.74	6
Ca	II	315.88	5.68	3.1	4
Ca	II	317.93	5.69	3.6	6
Ti	II	336.12	3.0	1.1	10
Ti	II	337.28	2.97	1.11	8
Sr	II	346.44	5.34	2.84	6
Ca	II	370.60	5.22	0.88	2
Ca	II	373.69	5.22	1.7	2
Fe	I	385.99	2.59	0.1	9
Sr	II	407.77	2.45	1.47	4
Sr	II	421.55	2.37	1.34	2
Ca	I	422.67	2.37	2.18	3
Ca	I	442.54	3.77	0.5	3
Ti	I	498.17	2.69	0.66	13
Ti	I	499.10	2.68	0.54	11
Ti	I	499.95	2.67	0.53	9
Ti	I	500.72	2.66	0.49	7

The analysis evidences that the LIBS spectra of the epoxy resin (segment 3 in sample N2-2 and segment 5 in sample S2-3) are very similar in the two samples, and the corresponding elemental composition obtained by the CF-LIBS analysis is very similar, as well (figures 7 and 8)

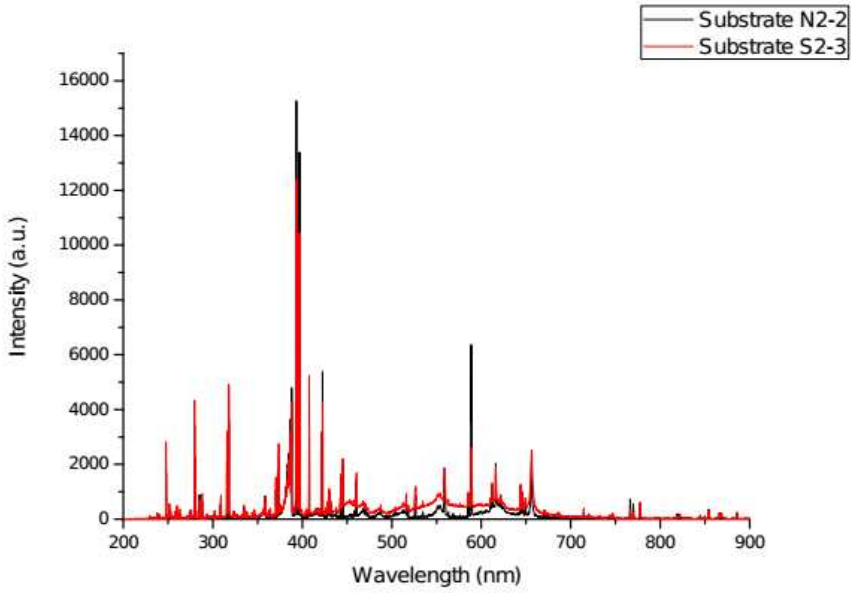

Figure 7 – Average LIBS spectra of the epoxy resin in samples N2-2 and S2-3

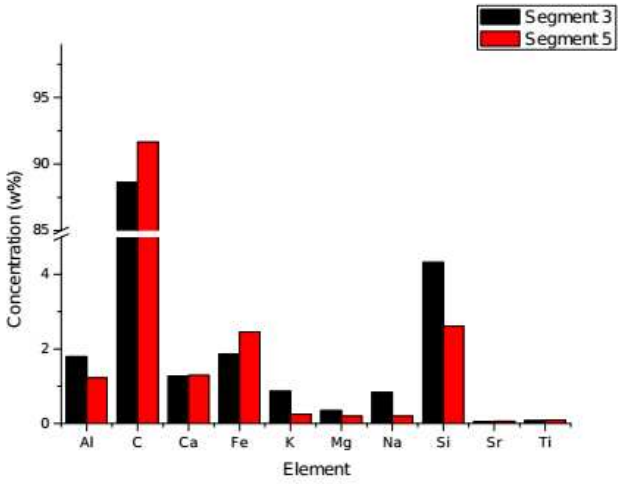

Figure 8 – Composition of the epoxy resin as determined by CF-LIBS in samples N2-2 (segment 3) and S2-3 (segment 5)

The composition of the other clusters is shown in figure 9, for the two mortar samples.

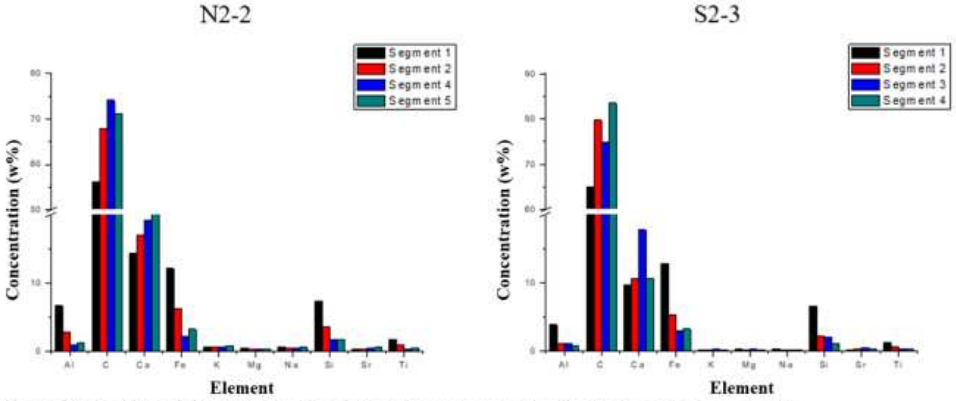

Figure 9. Results of CF-LIBS obtained for each segmented area *(excluding the epoxy resin)*.

Although the method presented is independent on the specific instrument used for the acquisition of the LIBS spectra, is worth to stress that, in our case, the LIBS spectra were acquired using a time-integrated spectrometer. Since the CF-LIBS method relies on the fundamental hypothesis of having the plasma close to Local Thermal Equilibrium [43], and this condition occurs in LIBS plasma only in a limited time interval, it might seem inappropriate its application to spectra which were acquired during the whole lifetime of the plasma. However, the authors have recently demonstrated that, due

231 to the fast decay of the LIBS signal in time, the acquired spectra are in fact dominated by the emission
232 of the plasma in a time window of about 1 μs [44]. In the time interval considered, typically the LIBS
233 plasmas are close to LTE conditions, and this consideration gives us confidence that the results
234 obtained are, indeed, meaningful.

235 The calculate electron temperature and number density are shown on top of the compositional map,
236 in figure 10. We see that the parts of the map where the epoxy resin was exposed are characterized
237 by hotter plasmas. This is a further occasion to note that whatever analytical method, applied to the
238 whole map, would have probably suffered the large differences in the matrix that characterize our
239 samples.

240

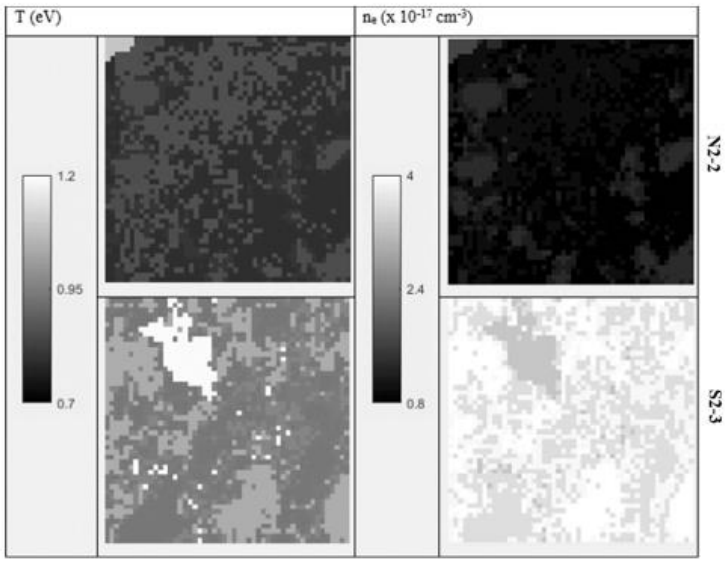

241

242 Figure 10 – Electron temperature and number density as calculated by CF-LIBS

243

244 From the data reported in figure 9, the quantitative compositional maps of the mortars can be obtained.
245 The most significant are shown in figure 11 (the epoxy resin was not considered).

246

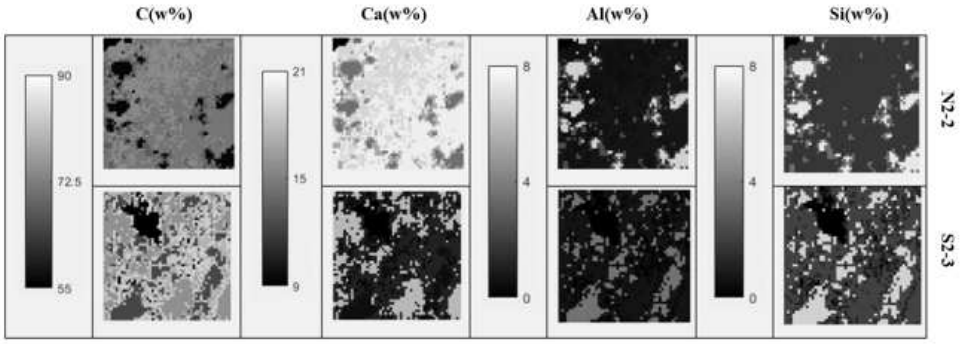

Figure 11 – Quantitative compositional maps of the two mortar samples (top: N2-2, bottom: S2-3)

The inspection of figure 11 shows that the method proposed in this paper, although not able to assess the fine compositional variations inside the different groups, provides results that reproduce well the texture of the samples. The comparison of the compositional maps obtained confirms quantitatively the differences between the two mortars that were already qualitatively evident from the visual inspection. The composition of the constituents of the sample can be obtained with a reasonable precision, typical of CF-LIBS analysis [45], of about ± 1% on the major elements and proportionally higher on the minor and trace elements, as evidenced in figure 8, where the same material (epoxy resin) was analysed in the two samples. We would like to stress once again that the high inhomogeneity of the samples would have made difficult any other quantitative approach based on global averages or comparison with reference samples. The CF-LIBS analysis has evidenced, in fact, large variations in the plasma parameters (electron temperature and number density, figure 10) within the same sample and between the two samples that can only be efficiently dealt with using a Calibration-Free approach.

4. Conclusions

We have proposed a fast method for the quantitative analysis of μ-LIBS elemental images, based on the application of the SOM method for the determination of the different classes of materials in the samples, followed by CF-LIBS analysis of the average representative spectra.

In this way, large variation of the sample matrix can be dealt with, and the textural features of the material can be obtained. The technique proposed is transportable, rapid and cheap. It has been presented and tested for the realization of compositional maps of historical mortar samples, but it could be easily applied to in situ analysis on modern building materials as well as, in general, to the analysis of highly inhomogeneous materials.

Acknowledgment
This work has been partially supported by MIUR (PRIN 2015 - 2015WBEP3H).

References

[1] J. Koch, D. Günther, Laser Ablation ICP-MS, in: F. Adams, S. Aime, L.A. Andersson, I. Ando, D.M. Andrenyak, D.L. Andrews, L. Andrews, S.R. Anthony, T.G. Appleton, C.M. Arroyo (Eds.), Encyclopedia of Spectroscopy and Spectrometry, Elsevier, 2010, pp. 1262-1269.

[2] A. Riedo, V. Grimaudo,P. Moreno-García, M.B. Neuland, M. Tulej, P. Broekmann, P. Wurz, Laser ablation/ionisation mass spectrometry: Sensitive and quantitative chemical depth profiling of solid materials, Chimia, (2016), 70 (4), 268-273.

[3] P.K. Diwakar, J.J. Gonzalez, S.S. Harilal, R.E. Russo, A. Hassanein, Ultrafast laser ablation ICP-MS: Role of spot size, laser fluence, and repetition rate in signal intensity and elemental fractionation, Journal of Analytical Atomic Spectrometry, (2014), 29 (2), pp. 339-346.

[4] L. Wang, L.Q. Yang, Y. P. Wang, L. Feng, X. Chen, Z.S. Chen, Developments of laser ablation inductively coupled plasma mass spectrometry (LA-ICP-MS) in microanalysis, Geological Bulletin of China, (2012), 31 (4), pp. 637-645.

[5] R. Uerlings, A. Matusch, R. Weiskirchen, Reconstruction of laser ablation inductively coupled plasma mass spectrometry (LA-ICP-MS) spatial distribution images in Microsoft Excel 2007, International Journal of Mass Spectrometry, (2016), 395, pp. 27-35.

[6] M.L.Warburton, M.R. Reid, C.H. Stirling, G. Closs, Validation of depth-profiling la-ICP-MS in otolith applications, Canadian Journal of Fisheries and Aquatic Sciences, (2017), 74 (4), pp. 572-581.

[7] K.E. Sjåstad, S.L. Simonsen, T. Andersen, Studies of SRM NIST glasses by laser ablation multicollector inductively coupled plasma source mass spectrometry (LA-ICP-MS), Journal of Analytical Atomic Spectrometry, (2012), 27 (6), pp. 989-999.

[8] O.T Butler, W.R.L. Cairns, J.M. Cook, C.M. Davidson, Atomic spectrometry update-a review of advances in environmental analysis, Journal of Analytical Atomic Spectrometry, (2017), 32 (1),pp. 11-57.

[9] Z. Qin, J.A. Caruso, B. Lai, A. Matusch, J.S. Becker, Trace metal imaging with high spatial resolution: Applications in biomedicine, Metallomics, (2011) 3 (1), pp. 28-37.

[10] P.J. Sylvester, LA-(MC)-ICP-MS trends in 2006 and 2007 with particular emphasis on measurement uncertainties, Geostandards and Geoanalytical Research, (2008) 32 (4), pp. 469-488.

[11] J.S. Becker, M. Zoriy, B. Wu, A. Matusch, J.S. Becker, Imaging of essential and toxic elements in biological tissues by LA-ICP-MS, Journal of Analytical Atomic Spectrometry, (2008) 23 (9), pp. 1275-1280.

[12] M.F. La Russa, C.M. Belfiore, V. Comite, D. Barca, A. Bonazza, S.A. Ruffolo, G.M. Crisci, A. Pezzino, Geochemical study of black crusts as a diagnostic tool in cultural heritage, Applied Physics A, (2013) 113 (4), pp. 1151-1162.

[13] B. Giussani, D. Monticelli, L. Rampazzi, Role of laser ablation-inductively coupled plasma-mass spectrometry in cultural heritage research: A review, Analytica Chimica Acta, (2009) 635 (1), pp. 6-21.

[14] J. Almirall, E. Cahoon, S. Jantzi, E. Schenk, T. Trejos, New developments in forensic applications of LIBS and LA-ICP-MS, Laser Applications to Chemical, Security and Environmental Analysis, (2012), LACSEA 2012

[15] J. Kaiser, M. Galiová, K. Novotný, R. Červenka, L. Reale, J. Novotný, M. Liška, O. Samek, V. Kanický, A. Hrdlička, K. Stejskal, V. Adam, R. Kizek, Mapping of lead, magnesium and copper accumulation in plant tissues by laser-induced breakdown spectroscopy and laser-ablation inductively coupled plasma mass spectrometry, Spectrochimica Acta B, (2009) 64 (1), pp. 67-73.

[16] B.T. Manard, C. Derrick Quarles, E.M. Wylie, N. Xu, Laser ablation-inductively couple plasma-mass spectrometry/laser induced break down spectroscopy: A tandem technique for uranium particle characterization, Journal of Analytical Atomic Spectrometry, (2017) 32 (9), pp. 1680-1687

[17] L. Sancey, V. Motto-Ros, B. Busser, S. Kotb, J.M. Benoit, A. Piednoir, F. Lux, O. Tillement, G. Panczer, J. Yu, Laser spectrometry for multi-elemental imaging of biological tissues Scientific Reports, (2014) 4, art. no. 6065

[18] L. Krajcarová, K. Novotný, M. Kummerová, J. Dubová, V. Gloser, J. Kaiser, Mapping of the spatial distribution of silver nanoparticles in root tissues of Vicia faba by laser-induced breakdown spectroscopy (LIBS)(2017) Talanta, 173, pp. 28-35

[19] N. Hausmann, P. Siozos, A. Lemonis, A.C. Colonese, H.K. Robson, D. Anglos, Elemental mapping of Mg/Ca intensity ratios in marine mollusc shells using laser-induced breakdown spectroscopy,Journal of Analytical Atomic Spectrometry, (2017) 32 (8), pp. 1467-1472.

[20] P. Fichet, J. Lacour, D. Menut, P. Mauchien, A. Rivoallan, C. Fabre, J. Dubessy, M.C. Boiron, micro LIBS technique, in: Laser-Induced Breakdown Spectroscopy: Principles and Applications, A.Miziolek, V.Palleschi and I.Schecter (eds.), Cambridge University Press ,2006, pp. 539–555.

[21] H. Bette, R. Noll, Laser induced breakdown spectroscopy at 1000 Hz with single pulse for high-speed, high-resolution chemical element mapping, Conference on Lasers and Electro-Optics Europe - Technical Digest, (2003), art. no. 1313540, 477

[22] K. Novotný, J. Kaiser, M. Galiová, V. Konečná, J. Novotný, R. Malina, M. Liška, V. Kanický, V. Otruba, Mapping of different structures on large area of granite sample using laser-ablation based analytical techniques, an exploratory study, Spectrochimica Acta B, (2008) 63 (10), pp. 1139-1144.

[23] C. Schiavo, L. Menichetti, E. Grifoni, S. Legnaioli, G. Lorenzetti, F. Poggialini, S. Pagnotta, V. Palleschi, High-resolution three-dimensional compositional imaging by double-pulse laser-induced breakdown spectroscopy Journal of Instrumentation, (2016) 11 (8), art. no. C08002

[24] R. Grassi, E. Grifoni, S. Gufoni, S. Legnaioli, G. Lorenzetti, N. Macro, L. Menichetti, S. Pagnotta, F. Poggialini, C. Schiavo, V. Palleschi, Three-dimensional compositional mapping using

double-pulse micro-laser-induced breakdown spectroscopy technique, Spectrochimica Acta B, (2017) 127, pp. 1-6

[25] E. Tognoni, G. Cristoforetti, S. Legnaioli, V. Palleschi, Calibration-Free Laser-Induced Breakdown Spectroscopy: State of the art, Spectrochimica Acta B, (2010) 65 (1), pp. 1-14

[26] A. Ciucci, M. Corsi, V. Palleschi, S. Rastelli, A. Salvetti, E. Tognoni., New procedure for quantitative elemental analysis by laser-induced plasma spectroscopy, Applied Spectroscopy, (1999) 53 (8), pp. 960-964

[27] T. Takahashi, B. Thornton, Quantitative methods for compensation of matrix effects and self-absorption in LIBS signals of solids, Spectrochimica Acta B, (2017) 138, pp. 31-42

[28] E. D'Andrea, S. Pagnotta, E. Grifoni, S. Legnaioli, G. Lorenzetti, V. Palleschi, B. Lazzerini, A hybrid calibration-free/artificial neural networks approach to the quantitative analysis of LIBS spectra, Applied Physics B, (2015) 118 (3), pp. 353-360.

[29] S. Pagnotta, M. Lezzerini, L. Ripoll-Seguer, M. Hidalgo, E. Grifoni, S. Legnaioli, G. Lorenzetti, F. Poggialini, V. Palleschi, Micro-Laser-Induced Breakdown Spectroscopy (Micro-LIBS) Study on Ancient Roman Mortars, Applied Spectroscopy, (2017) 71 (4), pp. 721-727

[30] F. Massazza, Pozzolana and pozzolanic cements, Lea's Chemistry of Cement and Concrete, (2003), pp. 471-635

[31] J. Válek, J.J. Hughes, C.J.W.P. Groot, Historic mortars: Characterisation, assessment and repair. A state-of-the-art summary, RILEM Bookseries, (2013) 7, pp. 1-12

[32] M. Lezzerini, M. Ramacciotti, F. Cantini, B. Fatighenti, F. Antonelli, E. Pecchioni, F. Fratini, E. Cantisani, M. Giamello, Archaeometric study of natural hydraulic mortars: the case of the Late Roman Villa dell'Oratorio (Florence, Italy), Archaeol. Anthropol. Sci., (2017) 9, pp. 603–615

[33] G. Gallello, M. Ramacciotti, M. Lezzerini, E. Hernandez, M. Calvo, A. Morales, A. Pastor, M. De la Guardia, Indirect chronology method employing rare earth elements to identify Sagunto Castle mortar construction periods, Microchemical Journal, (2017) 132, pp. 251–261.

[34] N. Li, N. Farzadnia, C. Shi, Microstructural changes in alkali-activated slag mortars induced by accelerated carbonation, Cem. Concr. Res., (2017) 100, pp. 214–226

[35] P. Ubbríaco, F. Tasselli, A Study of the Hydration of Lime-Pozzolan Binders, J. Therm. Anal. Calorim., (1998) 52, pp. 1047–1054

[36] C.M. Belfiore, G.V. Fichera, G. Ortolano, A. Pezzino, R. Visalli, L. Zappalà, Image processing of the pozzolanic reactions in Roman mortars via X-Ray Map Analyser, Microchem. J., (2016) 125, pp. 242–253.

[37] A. Bertolini, G. Carelli, F. Francesconi, M. Francesconi, L. Marchesini, P. Marsili, F. Sorrentino, G. Cristoforetti, S. Legnaioli, V. Palleschi, L. Pardini, A. Salvetti, Modì: A new mobile

instrument for in situ double-pulse LIBS analysis, Analytical and Bioanalytical Chemistry, (2006) 385 (2), pp. 240-247.

[38] P.A.Benedetti, G. Cristoforetti, S. Legnaioli, V. Palleschi, L. Pardini, A. Salvetti, E. Tognoni, Effect of laser pulse energies in laser induced breakdown spectroscopy in double-pulse configuration, Spectrochimica Acta B, (2005) 60 (11), pp. 1392-1401

[39] T. Kohonen, The self-organizing map, Neurocomputing, (1998) 21, pp. 1–6

[40] P.M. Atkinson, A.R.L. Tatnall, Introduction neural networks in remote sensing, Int. J. Remote Sens., (1997) 18, pp. 699–709

[41] T. Villmann, E. Merényi, B. Hammer, Neural maps in remote sensing image analysis Neural Networks, (2003) 16, pp. 389–403

[42] I.K. Fodor, A survey of dimension reduction techniques, Lawrence Livermore National Lab., CA (US), 2002

[43] G. Cristoforetti, A. De Giacomo, M. Dell'Aglio, S. Legnaioli, E. Tognoni, V. Palleschi, N. Omenetto, Local Thermodynamic Equilibrium in Laser-Induced Breakdown Spectroscopy: Beyond the McWhirter criterion, Spectrochimica Acta B, (2010) 65 (1), 86-95.

[44] E. Grifoni, S. Legnaioli, M. Lezzerini, G. Lorenzetti, S. Pagnotta, V. Palleschi, Extracting time-resolved information from time-integrated laser-induced breakdown spectra, Journal of Spectroscopy, (2014), art. no. 849310

[45] E. Tognoni, G. Cristoforetti, S. Legnaioli, V. Palleschi, A. Salvetti, M. Mueller, U. Panne, I. Gornushkin, A numerical study of expected accuracy and precision in Calibration-Free Laser-Induced Breakdown Spectroscopy in the assumption of ideal analytical plasma, Spectrochimica Acta B, (2007) 62 (12), pp. 1287-1302.